Actual path prediction and correction in tailored fiber placement process through a machine-learning algorithm

Composites Part C: Open Access 20 (2026) 100786

Contents lists available at ScienceDirect

Composites Part C: Open Access

journal homepage: www.sciencedirect.com/journal/composites-part-c-open-access

Actual path prediction and correction in tailored fiber placement process through a machine-learning algorithm

Eduardo A.W. de Menezes [a,*], Lars Bittrich [a], Patrick Schiebel [b], Andrea Miene [b], Leonel Echer [c,d], Mareike Woestmann [b], Axel Spickenheuer [a,e]

[a] Leibniz-Intitute for Polymer Research Dresden e. V. (IPF), Dresden, Germany
[b] Faserinstitut Bremen e.V. (FIBRE), Bremen, Germany
[c] SENAI Institute of Innovation in Polymer Engineering, São Leopoldo, Brazil
[d] Department of Structural, Geotechnical and Building Engineering, Polytechnic University of Turin, Turin, TO 10129, Italy
[e] Fakultät Design, Hochschule für Technik und Wirtschaft Dresden, Dresden, Germany

ARTICLE INFO

Keywords:
Machine learning
Tailored fiber placement
Image processing
Sensitivity analysis

ABSTRACT

Tailored Fiber Placement (TFP) is an additive manufacturing process for composite materials. It is based upon the embroidery technique, where continuous fiber rovings are positioned in a textile base material, fixed by a stitching yarn, and are later impregnated in a matrix. Its main advantage consists of the high design freedom, allowing the production of variable-axial reinforcements, depositing fibers only where desired and with optimized orientation. However, when dealing with small dimensions, deviations can be clearly observed between the target path (designed path) and the actual path, effectively stitched by the TFP machine. Among the sources for these deviations, one can mention fiber's waviness, buckling, materials involved, influence of input parameters, i.e., the tension applied at the roving, the distance between stitching points, speed, and other systematic deviations inherent to any manufacturing process. The present work focused on measuring these deviations and analyzing the influence of the stitching parameters on them. It was observed that the distance between stitching points plays a major role in this regard. After collecting the stitching data with varying inputs, a machine learning algorithm was trained to predict the deviations and to propose a second target path, whose objective is to minimize the deviations between the first target path and the actual path. The machine learning algorithm was able to minimize the average deviation over the target path by up to 55%.

1. Introduction

Unlike traditional materials, composites' mechanical properties are strongly dependent on the reinforcement orientation [1]. Furthermore, they are seldom applied in configurations such that all fibers are oriented in a unidirectional fashion [2]. Newer manufacturing processes aim to take advantage of their anisotropic behavior, allowing the design of variable-axial components, also referred to as fiber-steered composites or variable-stiffness laminates. By tailoring the reinforcement's angle, their structural performance can easily overcome conventional straight fiber laminates [3]. The usage of variable-axial composite significantly increased in recent years, in both academia and industry, with the most common fiber placing techniques being Automated Fiber Placement (AFP) [4,5], Continuous Tow Shearing (CTS) [6,7], and Tailored Fiber Placement (TFP) [8,9]. The latter, illustrated in Fig. 1, consists essentially of stitching a single fiber roving, in any direction of a 2D plane over a base material, where a double-locked stitch with upper and lower threads performs a zigzag pattern to fix the roving into this base material [10,11]. Advantages of TFP include higher out-of-plane mechanical properties, small curvature radius (≥5 mm), high reproducibility, productivity, and deposition speed [3,12–14]. The drawbacks include waviness or local roving buckling produced during the stitching [15].

Despite the high accuracy of TFP machines when pricking the holes to place the sewing thread, the fiber roving is not directly tied to the base material and has the freedom to move inside the boundaries established by the sewing thread. Therefore, the fiber roving does not strictly follow the designed path, especially in adverse conditions, such as small radii curves, where it tends to accumulate in the inner radius, decreasing the roving width and increasing the roving thickness [12]. This issue could

* Corresponding author.
E-mail address: menezes@ipfdd.de (E.A.W. de Menezes).

https://doi.org/10.1016/j.jcomc.2026.100786

Available online 29 July 2026

be circumvented by shortening the stitching length L (distance between two consecutive stitching points, measured parallel to the roving). However, it will increase the manufacturing time and produce composites with higher sewing thread content, and consequently less fiber volume. It has been shown [16] that L can significantly change the mechanical properties of unidirectional plates produced by TFP. Adjusting the zig-zag width Z (distance between two consecutive stitching points, measured perpendicular to the roving) to match the roving width is also an alternative to reduce deviations. However, differences in the roving shape, yarn spreading, and twists over the spool may result in segments lying outside the sewing thread boundaries when it is too tied. In general, industries aim for high production volumes in the shortest possible time. This drives the use of large stitching lengths (L) and high stitching speeds (S), which, however, tend to increase the deviations between the target path, defined in the CAM software, and the actual path, effectively stitched by the machine. Before the resin impregnation takes place, the preforms produced through TFP are usually stacked [17,18], similarly to traditional composite laminates, making the abovementioned deviations propagate throughout the part thickness. The process of digitalization, modeling of digital twins, and simulation of the parts' mechanical behavior at the mesoscale level are also strongly impacted by the features mentioned above [19].

In this context, the present work aims to build a machine learning (ML) algorithm to predict the actual path based on the target path. A supervised regression is used to learn a mapping from (i) local target-path geometry and (ii) process parameters to the measured roving deviation and width. The objective is not to propose a novel learning algorithm, but to establish a reproducible data pipeline and a correction workflow that can be deployed for TFP to reduce systematic placement error. It provides a self-optimization procedure, can handle complex and nonlinear data with many variables, and is capable of processing unstructured data. Moreover, ML relies on the data itself rather than on human-designed models, enabling the discovery of patterns that researchers might otherwise overlook, without being constrained by rigid assumptions [20–22]. The drawbacks are a higher dependency on data quality, poor performance in extrapolating, and usage of black-box algorithms, making it difficult to visualize the computed correlations [23–25]. Therefore, an experimental campaign is carried out to generate sufficient data and enable the algorithm to accurately predict the fiber roving position and width over a given path based on input parameters, namely, Z, S, L, and roving material. Subsequently, the algorithm is applied to create a corrected path, whose objective is to minimize the deviations between target path and actual path. To mitigate the influence of variables not employed as inputs in the ML algorithm, e.g., temperature, humidity, level of roving's yarns spreading, and roving tension, a second corrected path designed and applied during the stitching process, i.e., an updated corrected path is also proposed, thus it could adapt itself to the local conditions.

2. Materials and methods

2.1. Definition of the training track and materials

A training track, shown in Fig. 2, was designed to feed the ML algorithm with training data to elaborate a prediction model and, subsequently, to compute a corrected version of the target path. Its geometry consists of a collection of straight segments, 90° curves, arcs of different radii ranging from 15 mm to 50 mm approximately, sharp edges, spline segments, and a spiral, designed to cover a wide range of stitching possibilities in the shortest possible space. The stitching process begins at the green arrow and ends at the red arrow (see Fig. 2). The target path, followed by the roving, corresponds to the blue line, while the path followed by the sewing thread is the red line, and the red dots are the places for the stitching holes. The dimensions of the training track (neglecting the sewing thread) are 280 mm in width and 186 mm in height. The configuration depicted in Fig. 2 was adopted as default for several analyses conducted in this study. The zig-zag width Z and stitching length L (illustrated in Fig. 2) are 3 mm and 4 mm, respectively, while the stitching speed S is 600 stitches/min. The applied materials were a carbon fiber roving (CR), HT 800 tex, and a polyester multifilament sewing thread, 168 dtex. To avoid the potential large shearing in the woven, intrinsically related to the stitching process, A3 paper (80 g/m²) was applied, since it can be easily kept flat during the stitching process. The higher friction coefficient between this paper and the fiber roving in comparison to most woven fabrics also helps keeping it at the designated position. In addition, it allows for an easy identification of stitching holes. Another requirement for a successful post-processing analysis is a good color contrast between the roving and the base material. Therefore, the green color was selected for the A3 paper, yielding high contrast with both fibers used in this work, i.e., carbon (black) and glass (white). Therefore, two training tracks could be vertically stacked in the same A3 paper (297 mm × 420 mm), leaving a board wide enough to fit the sewing thread. All the samples were stitched in a Tajima TFP machine model TCWM-T01.

2.2. Comparison between target path and actual path

The stitched samples were scanned in a Toshiba flatbed scanner (600 DPI) using blue A3 paper on the background to increase the contrast between the stitching holes and the green paper. A scanned image obtained after stitching with the default configuration, using the stitch file from Fig. 2, is shown in Fig. 3. Later, the image processing procedure takes place to evaluate the actual path. The first processing step is the alignment between the scanned image data and the data extracted from

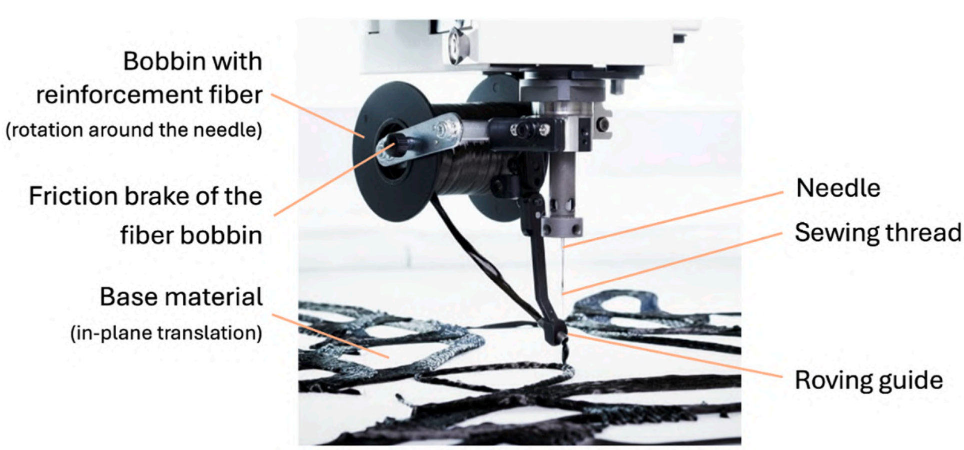

Fig. 1. Stitching process of a TFP preform, showing a carbon fiber roving being stitched over a base material (glass woven).

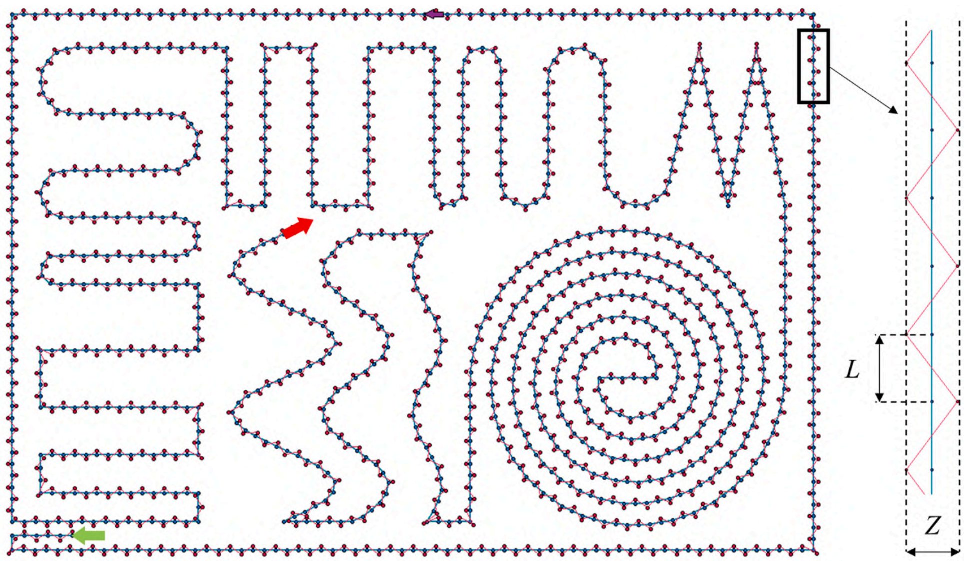

Fig. 2. Training track modeled in the software EDOpath with default inputs, applied to generate the data for feeding the ML algorithm.

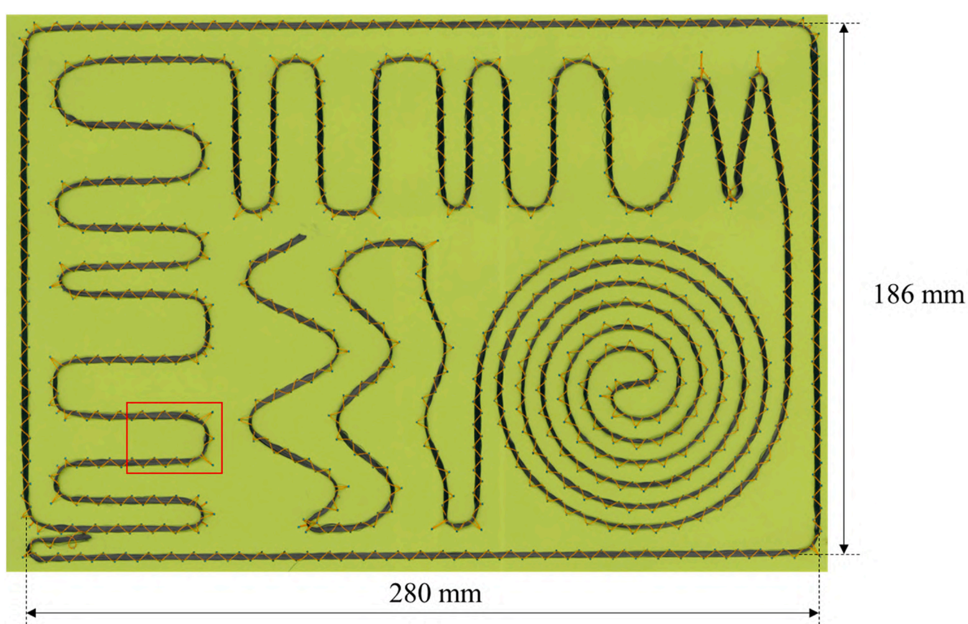

Fig. 3. Scanned image obtained from the default configuration.

the training track file (shown in Fig. 2). Since the stitched sample has to be taken out of the TFP machine for scanning, the positioning system of the machine cannot be used in this step. Slight rotation of the sample during scanning might occur as well and has to be corrected before any further analysis. After calibrating the scanner, it is possible to transfer the coordinates from the image coordinate system, which uses pixels and has its origin in the upper left corner, to the coordinate system of the stitch file, which uses millimeters and has its origin in the lower left corner. After correcting the rotation, the offset between them is computed and corrected.

The next step comprises a color-based segmentation. To illustrate this process the segment from the training track within the red rectangle, shown in Fig. 3, is magnified in Fig. 4(a). The identification of stitch holes, roving, and sewing threads are shown in Fig. 4(b), Fig. 4(c), and Fig. 4(d), respectively. As can be seen, the roving is incomplete, since it is partially covered by the sewing thread. A morphological closing operation is carried out (see Fig. 4(e)) and, subsequently, a polygonal approximation is applied to define the roving contour, depicted in Fig. 4 (f), which is employed to compute the roving width.

From the roving contour, a one-pixel wide centerline is established using morphological operations, which is reduced to a sequence of points. This centerline, depicted in Fig. 5, defines the actual path. A Python script was elaborated to synchronize the data from the target path and actual path. This was accomplished by normalizing the distance between data acquisition in the actual path as a function of the total placement length and then splitting it into intervals defined by the data from the target path. Therefore, it was possible to mitigate deviations due to mismatches in the direction parallel to the roving. The second step consists of taking each measurement from the actual path and detecting the equivalent one in the target path. Due to the excessive deviations presented in some configurations, this process could not be done by solely searching for the closest point. It was required to search within a given placement window frame inside the vicinity of the given point. Next a two-dimensional vector linking these two points is

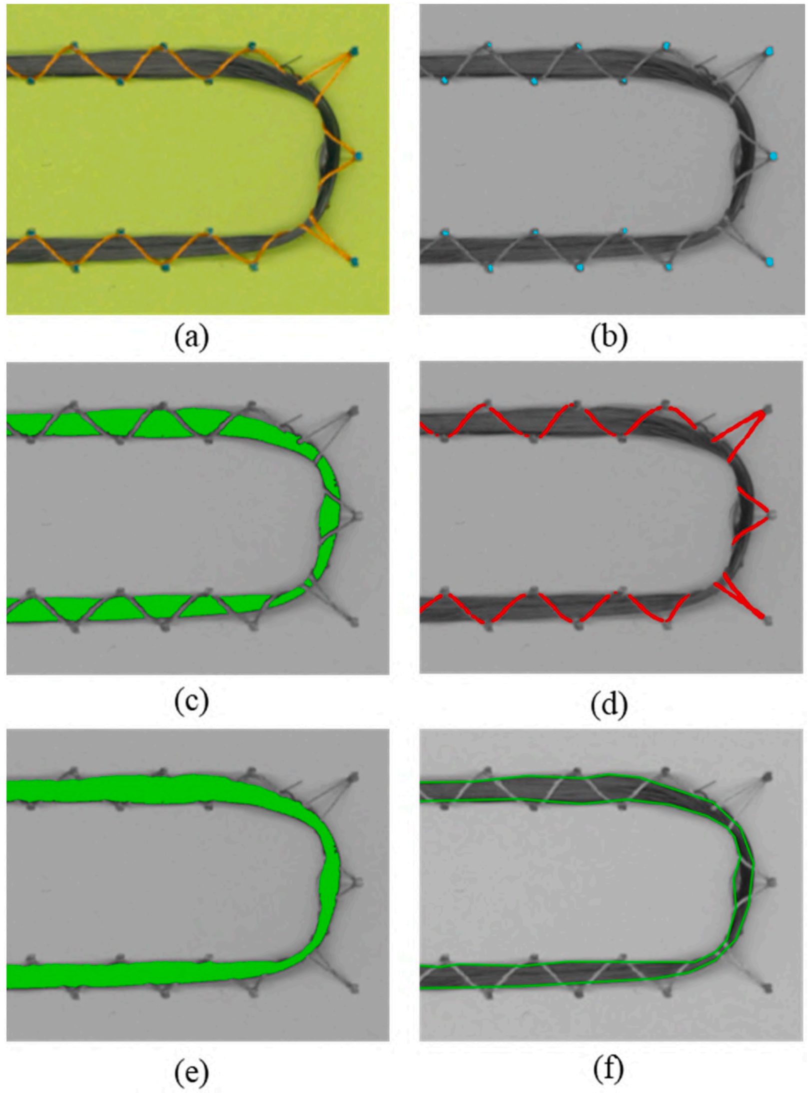

Fig. 4. (a) Roving segment extracted from Fig. 3, (b) stitch holes segmented in blue regions, (c) monochrome region segmented in light green, (d) sewing thread segmented in red regions, (e) roving segmented in light green, and (f) polygonal approximation of roving contour.

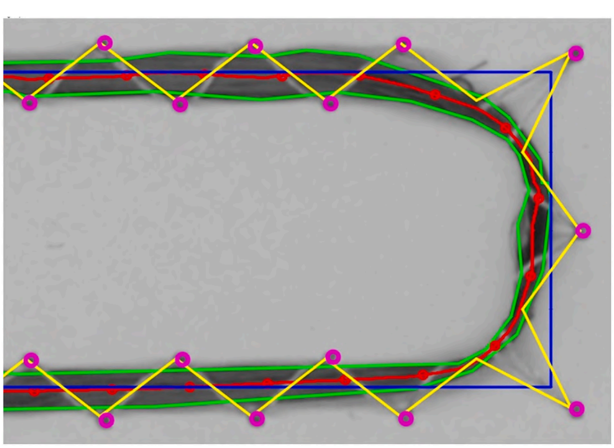

Fig. 5. Identification of the roving's contour (green line), centerline (red line), and stitch holes (pink dots), showing also the target path (blue line) and sewing thread (yellow line).

established, whose magnitude corresponds to the deviation between them. The cross product between this vector, and a vector parallel to the roving (considering the target path) defines if the deviation is either positive or negative (to the right or the left of the placement direction, respectively).

2.3. Experimental campaign

To provide the ML algorithm with sufficient data for predicting and correcting the target path, an extensive experimental campaign was carried out, where the training track, shown in Fig. 2, was repeatedly stitched with varying input parameters. Three different types of roving were applied: CR with 800 tex (HT) and 1600 tex (HT), and glass fiber roving (GR) with 1200 tex. For design purposes, the value of Z should not be too low and cause the roving fibers to be partially outside the sewing thread, nor too high that the roving is loose. Therefore, it is not necessary to investigate a wide range of this property. The training track was stitched using $Z = 2.0$ mm, 3.0 mm, and 4.0 mm.

Regarding S, from the industrial point of view, it is desirable to investigate the behavior at the machine's maximum speed (1000 stitches/min). However, it was observed that for speeds above 600 stitches/min, the machine automatically decreases it when stitching the curved segments of the training track, which would create invalid comparisons. Hence, the applied values for S were 400 stitches/min, 500 stitches/min, and 600 stitches/min, so the machine could keep it constant. Relative to L, higher values allow quicker manufacturing, lowering also the volume of the sewing thread in the final part. On the other hand, lower values reduce fiber waviness and increase the accuracy in the roving position. The applied values were 2 mm, 4 mm, 6 mm, and 8 mm. It is noteworthy to highlight that the stitching points were forced to be placed in the corners of the right angles of the training track, so the actual values of L may deviate from the given inputs. Although these deviations were generally small, at few specific locations it was larger, reaching values up to 25 % of the set value. This was done to keep a fair comparison for configurations with different L values. Additionally, the training track was also stitched with random values between 1 mm and 7 mm to enhance the learning capabilities, since this parameter should not be treated as a constant throughout the process and typical preforms exhibit changing L throughout the process.

To investigate also the cross-influence between these variables and improve the prediction's accuracy, all possible combinations of the values above were stitched. Therefore, considering three different rovings, three values for S, three values for Z, and six values for L (two random samples were generated for each combination), a total of $3 \times 3 \times 3 \times 6 = 162$ training tracks were manufactured.

Another crucial parameter to be investigated is the roving tension during the stitching process. However, it cannot be directly controlled as the other input variables mentioned earlier in the TFP machine applied here. Instead of a constant force, a constant torque is applied to the roving bobbin. Therefore, the tension force in the roving is a function of the bobbin's mass, frictions, and radius (6 mm when empty and approximately 25 mm when filled with roving). Since the rovings have a low density, and the friction is constant during the process, only the radius variation is expected to significantly change the roving's tension. Hence, the deviations between target path and actual path are also investigated by comparing bobbins at their full stage (larger radius) and at their almost empty stage (smaller radius), for both roving and sewing thread bobbins, using the default configuration.

2.4. Machine learning model and training

For each experiment depicted in Section 2.3, stitch coordinates were transformed into local, stitch-centered representations using a sliding window approach, in which relative in-plane displacements over neighboring stitches were used as input features. These geometric descriptors were augmented by normalized process parameters (Z, machine speed, and production angle) to form the final feature vector $x \in \mathbb{R}^d$. Targets comprised the measured in-plane deviations between target and measured roving position and local roving width, scaled for numerical stability to form outputs $y \in \mathbb{R}^3$. Fully connected feedforward neural networks with 5 hidden layers (20 nodes per layer, GELU activation) were trained using the Nadam optimizer and mean squared error loss [20]. The learning rate $\eta = 0.001$ and standard exponential decay parameters were used with a mini-batch size of 128 samples to balance gradient stability and computational efficiency. To ensure reproducibility of the validation split and stochastic training effects, a fixed random seed was applied to the NumPy random number generator prior to data partitioning. Each configuration was trained multiple times to account for residual stochastic variability arising from weight initialization and mini-batch sampling. A systematic design of experiments was applied to vary window size, network depth, width, and the inclusion of a zig-zag position index feature i.e. whether the roving is left or right of the stitches, and each configuration was trained repeatedly to account for stochastic effects. Model performance was evaluated using a hold-out validation strategy. For each experimental dataset, 20% of the eligible stitch positions were randomly selected and reserved exclusively for validation prior to training. The split was performed at the stitch level after construction of the sliding-window features to ensure that validation samples were not used during parameter optimization. Early stopping was applied based on the validation loss with a patience of 20 epochs, and the model weights corresponding to the minimum validation loss were restored. This procedure provided an unbiased estimate of generalization performance while mitigating overfitting. Convergence of model performance was observed for >4 layers, >15 nodes per layer, and at least 7 stitches in the stitch window. The zig-zag position index had no significant predictive impact on the output performance. This approach enabled a quantitative mapping between process parameters and local placement deviations, providing a basis for improving TFP production accuracy.

2.5. Correcting procedure through ML

The subsequent step consists of generating a corrected stitch path by iteratively updating the target path $\left(\tilde{x}_i, \tilde{y}_i\right)$ based on the deviations predicted by the trained machine learning model. The objective is to minimize the discrepancy between the corrected stitch path and the original (not updated) target path (x_i, y_i), while accounting for the systematic placement errors learned by the model.

Using the trained surrogate model $M\left(\tilde{x}_i, \tilde{y}_i\right)$, which predicts the local deviation vector between stitch and roving position, the actual roving position can be approximated as the sum of the corrected stitch coordinates and the predicted deviation. The corrected path is obtained by solving the nonlinear least-squares problem

$$\min_{\left(\tilde{x}_i, \tilde{y}_i\right)} \sum_i \| M(\tilde{x}_i, \tilde{y}_i) + (\tilde{x}_i, \tilde{y}_i) - (x_i, y_i) \|^2,$$

thereby minimizing the squared Euclidean distance between the predicted actual roving position and the nominal target path. Gradients obtained from the differentiable neural network model were exploited to accelerate convergence of the optimization procedure.

Two distinct correction strategies were investigated.

Forward strategy:

In the forward formulation, the nominal stitch path is used as input to the trained model, which predicts the expected roving deviation. The stitch positions are then iteratively adjusted such that the predicted actual roving path approaches the desired nominal path. This approach directly solves the above least-squares problem using the forward surrogate model.

Inverse strategy:

In the inverse formulation, the training data are restructured to learn the inverse mapping. A second model M_2 is trained to predict corrected stitch positions directly from prescribed roving positions. By prescribing the nominal roving path as input, the model outputs the stitch path that is expected to produce this trajectory during manufacturing. This strategy therefore avoids iterative optimization and provides a direct prediction of corrected stitch coordinates.

Both approaches enable model-based compensation of systematic placement errors within the TFP process, either through gradient-based optimization (forward method) or direct inverse regression (inverse method).

Given the influence of variables not incorporated as inputs during the training, mentioned in Section 1, a real-time training is proposed to enhance the prediction's accuracy. The idea is to simulate a practical application, where the algorithm identifies the local conditions and then dynamic changes on the predictions to adapt itself and improve them still during the stitching process. For that purpose, a first training track is stitched, using the target path. This track is then immediately scanned, and the prediction model is updated with the results from the actual path, so a second training track is stitched using the updated corrected path. For this renewed training the previous best model weights are loaded and the model then is trained only on the new data, which is very fast, but completely disregards previous experience except for a good initial condition. This sequential stitching aims to minimize the effect of local changes since the TFP machine remains static during the scanning and re-training and is applicable to a complete change in material that was not seen in the training. In terms of practical applications, it should also enhance the training performance for different materials or stitching parameters not incorporated in the original training.

3. Results and discussion

A preliminary analysis was made after stitching the training track with the default configuration (CR, 800 tex, $S = 600$ stitches/min, $Z = 3$ mm, and $L = 4$ mm) three times, where the results for the deviation between target path and actual path from one of them are plotted in Fig. 6. The actual path consists of black circles connected by a black line, while the points of the target path are plotted in a diverging colormap. Results are also plotted as a function of the roving's width in Fig. 7 and as a function of the deviation in the roving's orientation angle in Fig. 8. The orientation angles are computed in the segments between two adjacent stitches.

Considering the three samples, the average deviation was 0.734 mm $\pm$0.013 mm, and the median was 0.478 mm $\pm$ 0.021 mm. The reproducibility observed here was very high, and a median value lower than the average indicates that the lower values dominate the measurements with fewer but higher exceptions. For a better analysis and discussion of the results presented above the training track was virtually split into seven different regions, illustrated in Fig. 9. The deviations regarding the roving's position for each one of them are shown in Table 1.

Region 1 (gray) lies at the beginning and at the end of the training track (as defined in Fig. 2). In the beginning, the roving was not properly fixed yet, and it tends to stay out of the limits defined by the sewing thread in some cases. In the final part, the roving is loose and can easily change its orientation with small movements when cutting it from the spool. Therefore, the values computed from Region 1 were excluded from the data and error analysis performed in this work. To not impact the scaling of the color plots, it was also suppressed from Figures Fig. 6, Fig. 7, and Fig. 8
Region 2 (blue) consists of the four long straight segments. Deviations in the roving position were negligible, which can be clearly observed in Fig. 8, where a value close to 0° is computed over it. Fig. 7 shows also that an approximately constant width is measured in this region, unlike the other ones.
Region 3 (green) consists of the quarter-arcs (90° curves forming right angles) found in two separate places. As expected, a high deviation in the roving position is observed there, which is highlighted when observed as a function of the angle in Fig. 8. Fig. 7 also shows the roving's tendency to accumulate in the inner radius of these curves, reducing its width and, consequently implied, increasing its height.
Region 4 (violet) is formed by the two subregions with half-arcs (180° curves with constant radius). Here the deviations are also high, but slightly lower than Region 3. A smoother distribution in comparison with the quarter-arcs can be observed for both deviations in position and angle, and the width reduction is also observed.
Region 5 (red) contains V-shape sharp edges and presented the highest observed deviations. In Fig. 7 it is possible to see a point where a superposition of two rovings occurred, and the image processing grouped them as one to compute the width. Fig. 3 shows that the roving could not even be kept inside the limits defined by the sewing thread in two of the three tips.
Region 6 (aquamarine) is a spiral formed by a collection of 180° arcs. The arcs have a constant curvature radius, whereas the outer arcs have a higher radius, decreasing while approaching the center. It is interesting to observe, from Fig. 6, how the deviations are low in the outer arcs, but significantly increase when the curvature radius decreases, in the inner arcs. Regarding width distribution, one can observe variances inside the spiral due to the roving's twisting movement, changing its value with no established pattern. Region 2 already shows some variation in the roving's width due to the manufacturing process, even without twisting. However, they are smaller than the ones observed in Region 6, where the effects of width variation due to manufacturing and twisting sum up. Deviations relative to the angle could not be observed in the spiral. As in regions 3 and 4, the roving tendency to deviate from the target path, by moving to the inner radius of the curves, limited by the stitching points, could be observed.
Finally, Region 7 (orange) consists of a set of spline segments, with no constant radius and concavities in interchanging directions. Deviations in the position could only be observed on the top of the concavities, while due to the changes in the radius deviation in the angle between actual path and target path happened throughout the splines. The lack of straight segments in Region 7 caused its average deviation to be comparable with the deviations measured in Region 5.

Fig. 9 shows also many black points connecting different regions or segments of the same region. These points inside transition regions were not incorporated in any region from 1–7, but they were considered when

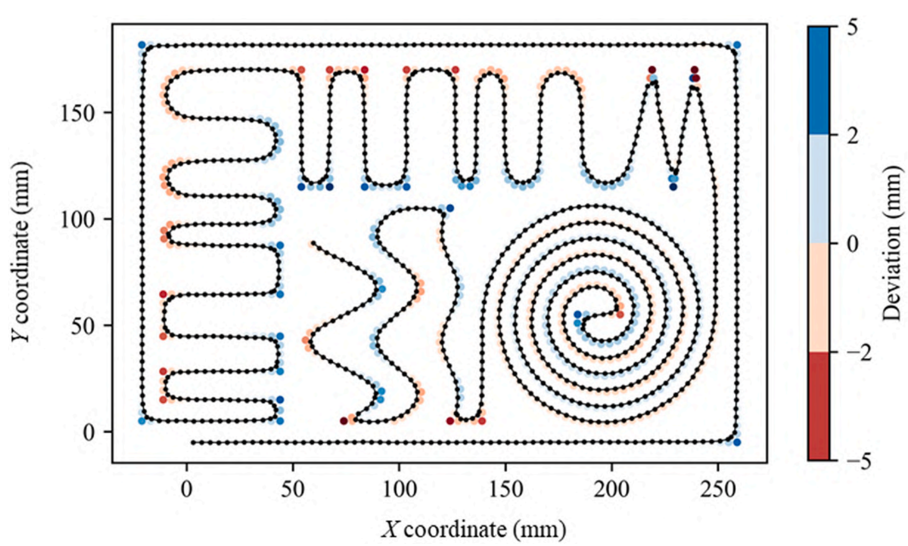

Fig. 6. Deviation between the coordinates of the target path and actual path obtained from a sample stitched with the default configuration.

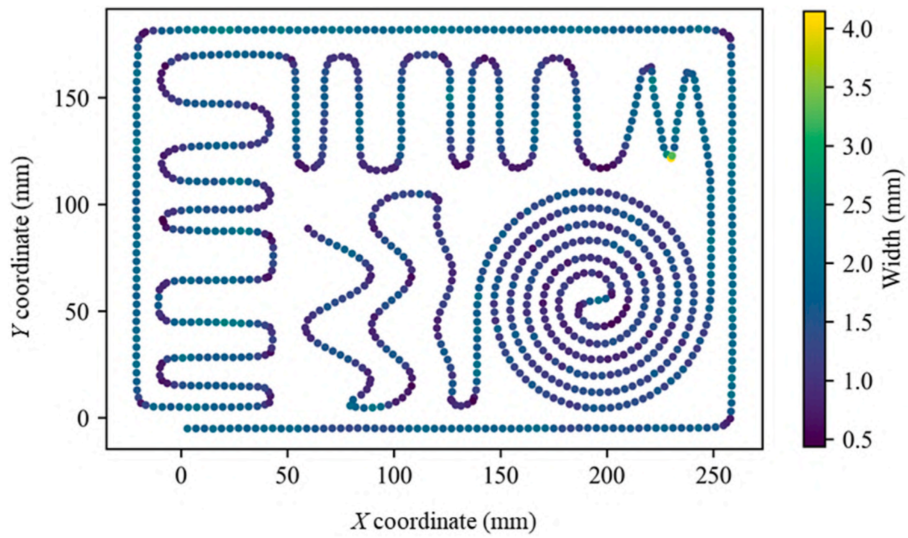

Fig. 7. Width of the fiber roving over the training track. The single yellow dot on the sharp edge, out from the 4 mm scale limit, refers to a measurement where two adjacent rovings were interpreted as one.

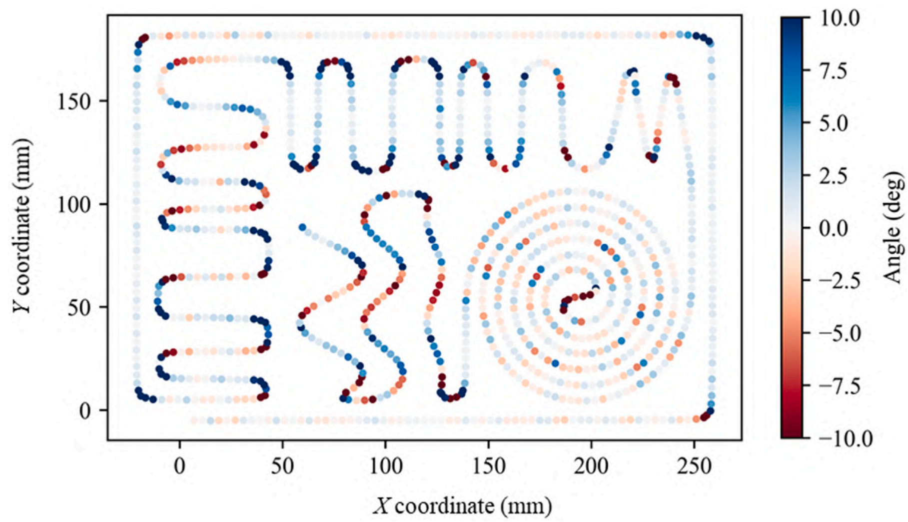

Fig. 8. Deviation between the roving's orientation angle of the target path and actual path.

computing the overall deviation.

Regarding the analysis of the systematic deviations, the results are plotted in Fig. 10. This graphic depicts the average deviations of all the samples (among the total of 162) stitched with the given parameter. Namely, the first column on the left reports the average deviation considering all samples manufactured with CR 800 tex, independently of the values applied for *S, Z*, and *L*).

The accuracy gain when switching from a smaller to a bigger roving (800 tex to 1600 tex) is explained by the lower freedom of the roving to move inside the limits defined by the sewing thread. The accuracy loss when switching from carbon to glass fibers could be explained by the higher friction coefficient of the latter [26], increasing the roving's spreading and torsion. However, this coefficient was not verified in the context of the TFP process here. The percentual differences between CR 800 tex and CR 1600 tex against GR 1200 tex were 5.0% and 17.0% respectively, indicating potential issues when extrapolating the training results to other roving materials other than glass or carbon.

Regarding the stitching speed *S*, the average deviation increased by 6.8% when it increased from 400 stitches/min to 500 stitches/min, and 14.7% when it increased from 500 stitches/min to 600 stitches/min. Therefore, it is clear that inertia effects play a significant role in the machine's accuracy.

Relative to the zig-zag distance *Z*, while the difference between 2 mm and 3 mm was negligible (0.9%), increasing it from 3 mm to 4 mm yielded a noticeably higher deviation (9.8%). This result was expected for the same reasons mentioned when increasing the roving volume since the roving becomes more constrained when *Z* decreases. However, when Z is increased, the roving tends to spread laterally, resulting in greater width and reduced height, since its cross-sectional area remains constant [12]. But this effect only takes place within a certain threshold, which probably at some point between 2 mm and 4 mm and might depend on the geometry of the feeding pipe that was kept fixed in this study.

From Fig. 10, it is clear that *L* plays a major role in the deviation between the target path and actual path output, and its impact on the accuracy is also illustrated in Fig. 11. Average deviations with 8 mm were almost four times higher in comparison to 2 mm. However, the accuracy gain when reducing *L* was not homogeneously distributed over the regions of the training track. In Region 2 the difference, in absolute values, was very low. In regions 3 and 4 a significant accuracy gain was

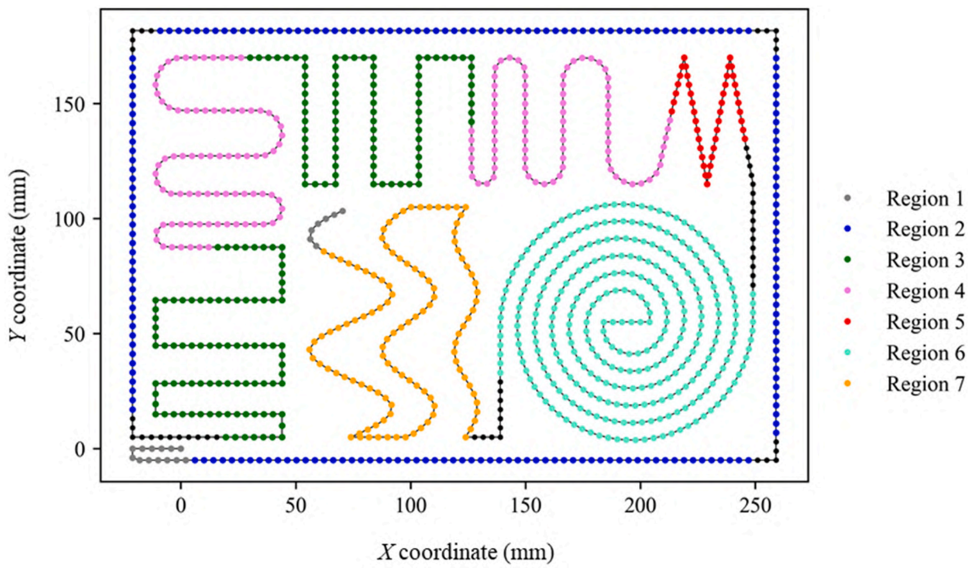

Fig. 9. Training track virtually split in seven different regions.

Table 1
Deviations between target path and actual path for the different regions of the training track, obtained with the default configuration.

Region	Sample 1		Sample 2		Sample 3	
	Max. (mm)	Avg. (mm)	Max. (mm)	Avg. (mm)	Max. (mm)	Avg. (mm)
2	0.655	0.154	0.519	0.085	0.825	0.151
3	5.236	0.972	4.535	0.915	4.821	0.844
4	3.187	0.807	3.421	0.849	3.158	0.868
5	7.320	0.886	9.032	1.186	8.400	1.159
6	3.970	0.791	4.409	0.842	4.042	0.792
7	5.504	1.061	5.485	1.081	5.516	0.999
Total	7.320	0.730	9.032	0.750	8.400	0.724

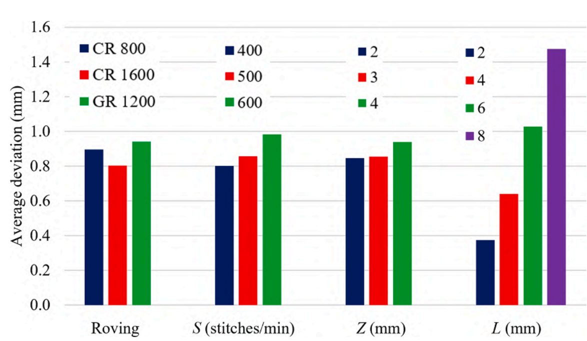

Fig. 10. Results of systematic deviations as a function of selected parameters.

observed, while in Region 5, even a low L could not avoid high deviations in the sharp edges. Region 6 was the one with the highest accuracy gain since it contains no straight segments. Region 7 contains a combination of sharp edges and splines with a high curvature radius, and, therefore, the accuracy gain there was not as high as in regions 3, 4, and 6. Since the manufacturing time in the TFP process is a function of the number of stitching points, this analysis indicates that it could be reduced by applying adaptive steering of L values, e.g., increasing it in straight segments and decreasing it as a function of the curvature radius.

Cross-influences could not be observed between Z and S. However, the deviations for $L = 2$ mm, and speed of 400 and 600 stitches/min were 0.382 mm and 0.377 mm, respectively. Although it was expected the lower speed to yield lower deviations, this 1.3% difference is small enough to be neglected given the approximations applied when computing these values. However, when computing the deviations for $L = 8$ mm and speeds of 400 and 600 stitches /min, the results were 1.335 mm and 1.673 mm, respectively (25.3% difference). Therefore, the influence of S is sensitive to the applied L, increasing as it increases. An opposite behavior was observed between Z and L. When $L = 2$ mm the deviations for $Z = 2$ mm and $Z = 4$ mm were, respectively, 0.312 mm and 0.465 mm (49.2% difference), while when $L = 8$ mm the deviations for $Z = 2$ mm and $Z = 4$ mm were, respectively, 1.479 mm and 1.483 mm (0.2% difference). Therefore, the influence of Z becomes smaller as L increases, which is reasonable, considering that the number of points over the training track that the sewing thread constrains the roving is reduced.

Given the limitation in stitches per minute of TFP machines, the production time is a function of the total number of stitches, which in turn depends on L, and S. Based on the relationships observed here, it is possible to design a compromise between these two input parameters and the resulting accuracy. For instance, production time can be minimized by defining a target accuracy and optimizing S and L to achieve this accuracy in the shortest time. Another possible strategy is to vary these inputs across the preform, e.g., reducing S and L in curved regions and in the vicinity of sharp edges, while increasing them in straight segments. Commercial TFP machines already have built-in functions to automatically lower the speed in certain regions, overriding the input value of S. CAM software (EDOpath) also includes algorithms to reduce L as a function of the curvature radius. Although the qualitative need for such parameter variations is well known, the quantitative analysis presented here serves as a design guideline to tailor these parameters and enhance existing approaches for balancing process inputs and accuracy.

As explained in Section 2, a different force is applied by the machine to unwind their respective bobbins whether they are almost empty or full, due to the radius change and a torque controlled by constant friction force at the bobbin. Its influence relative to the roving's bobbin on the deviation between the target path and actual path was quantified by stitching 20 training tracks using the default configuration, where 10 training tracks applied a full bobbin and 10 training tracks applied an almost empty bobbin. The full bobbin yielded an average deviation of 0.652 mm ± 0.027 mm, while the almost empty yielded 0.747 mm ± 0.039 mm (an increase of 14.6%). A statistical analysis through Welch's t-test [27] could show, with a significance level of 2.5% (two-tailed), that the families are indeed different. It is important to highlight that both families were stitched sequentially.

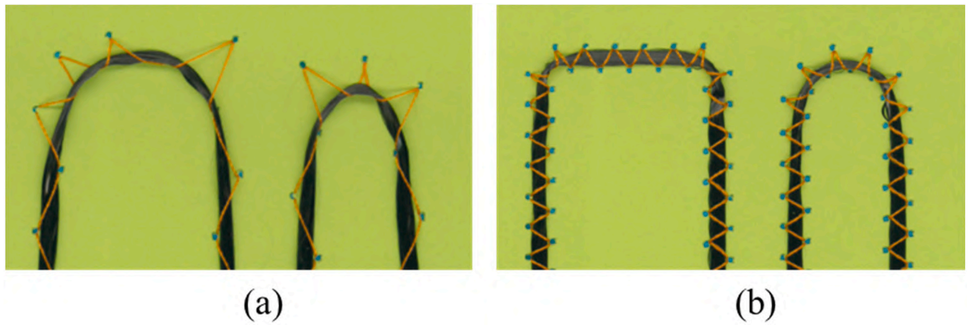

Fig. 11. Segment of a 180° arc and two right-angle curves from training tracks stitched with (a) $L = 8$ mm and (b) $L = 2$ mm, constant Z and S.

A similar test was conducted regarding the bobbin with the sewing thread, where 12 training tracks were stitched with full bobbin and 22 with almost empty bobbin, also with the default configuration. While the training tracks with full bobbin yielded a deviation of 0.687 mm $\pm$ 0.018 mm, when almost empty the average deviation was 0.628 mm $\pm$ 0.029 mm. Even with closer values, when compared to the roving bobbin, Welch's *t*-test also points to statistical differences between them. However, this time an empty bobbin increased the accuracy. While the position of the sewing thread does not have a direct impact on the roving's position, excessive tension could lead to shrinkage and wrinkles in the base materials, leading to accuracy loss.

After analyzing all the earlier mentioned samples, the prediction model could be implemented, and the results for the default configuration are shown in Fig. 12. As can be seen, the red line with red circle markers, containing the prediction model, tends to follow the dots with black contour (actual path), even in the situation where it significantly deviates from the blue line (target path)

The last step consists of building the corrected path and the updated corrected path, which was done for the default configuration and for $L =$ 8 mm, with the other variables as in the default one. The results are reported in Fig. 13 and illustrated in Fig. 14. As can be seen, the corrected path showed a huge accuracy gain for both the forward method and the inverted method. Deviations were also reduced after implementing the updated corrected path, highlighting the role played by local effects and variables not directly inserted into the prediction model. Although the accuracy increased approximately in a proportional fashion for the configurations with $L = 8$ mm and $L = 4$ mm, in absolute values the deviations got closer. The tendency of producing deviations homogeneously distributed through the training track, induced by the least squares method, can be observed in Fig. 14. When approaching a curved segment, the strategy adopted is to slightly deviate to the opposite side right before the curve, increasing the deviation there, but significantly reducing it along the curve.

4. Conclusions

A training track was designed, incorporating a variety of geometries, enabling the identification of the accuracy of the stitching process under different circumstances. A digitalization procedure to analyze the actual path produced from a given target path was established, allowing the subsequent quantitative analysis of the deviations between them. Using the training track proposed several input parameters were investigated relative to their influence on these deviations. From there, it became obvious that the stitching length was the most relevant parameter. Cross-influence between the parameters was also found. Later, a prediction model was elaborated using a machine learning algorithm, fed from the experimental campaign conducted on the training track. This prediction model allowed a correction algorithm, based on least squares optimization, to be applied for designing a corrected path, whose objective was to minimize the deviations from the target path. Deviations were reduced by around 42.5%. After performing another evaluation, based on deviations measured right before the testing, and then feeding the optimization algorithm with these measurements, deviations could be reduced by around 50.5%, since it could adapt itself to

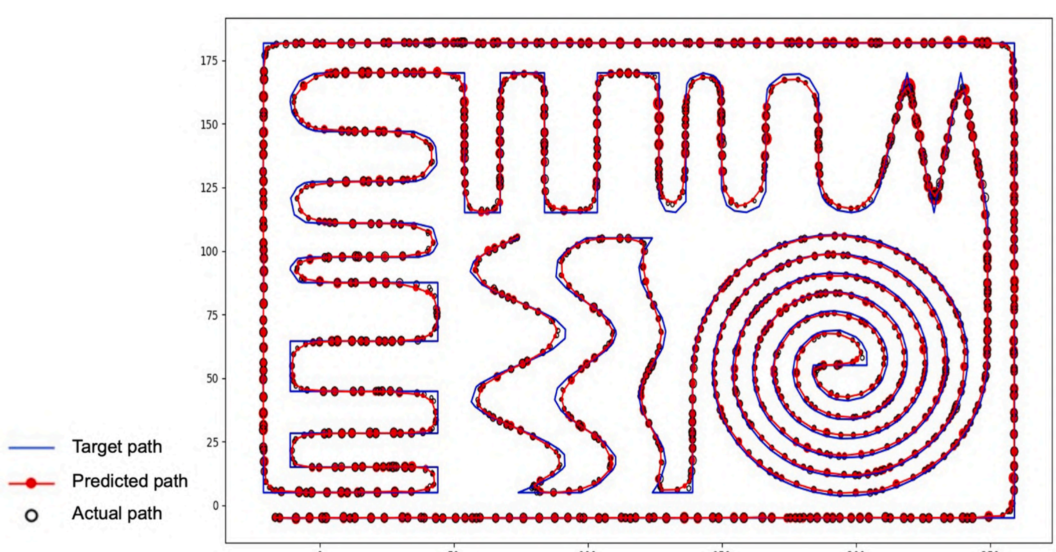

Fig. 12. Target path (blue line), predicted path (red line with red dots), and actual path (dots with black contour). The size of the dots is inversely proportional to the accuracy of the prediction model.

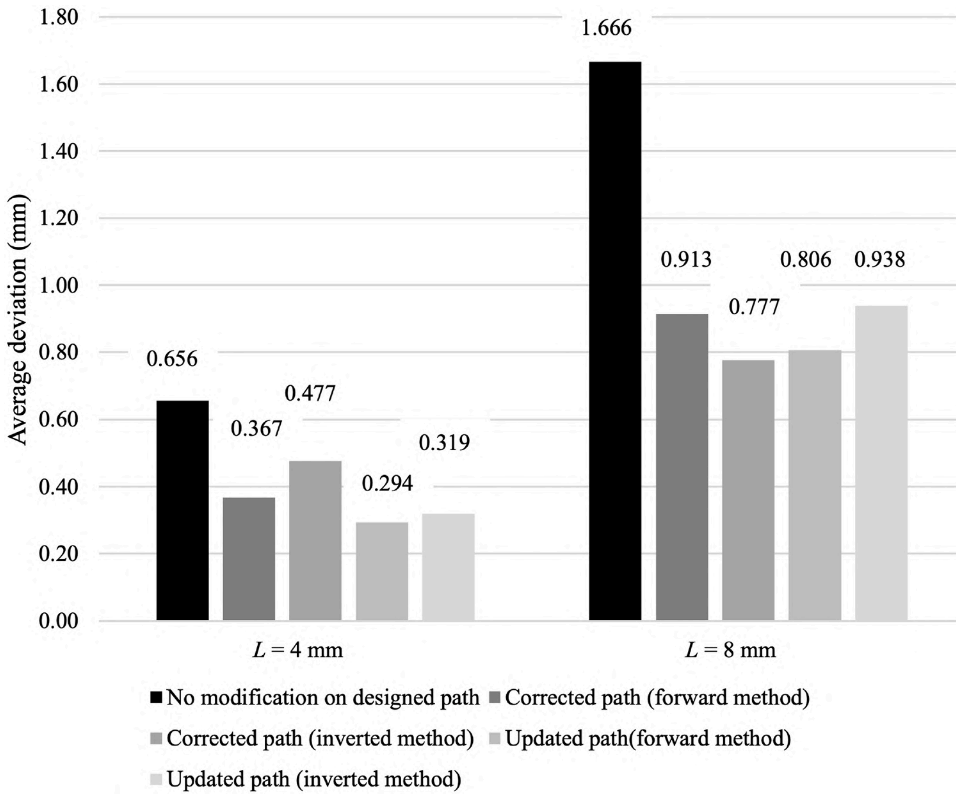

Fig. 13. Average deviation on a training track with default configuration (L = 4 mm) and L = 8 mm, before and after implementing the corrected path and updated corrected path. Actual values are displayed in the top of each column.

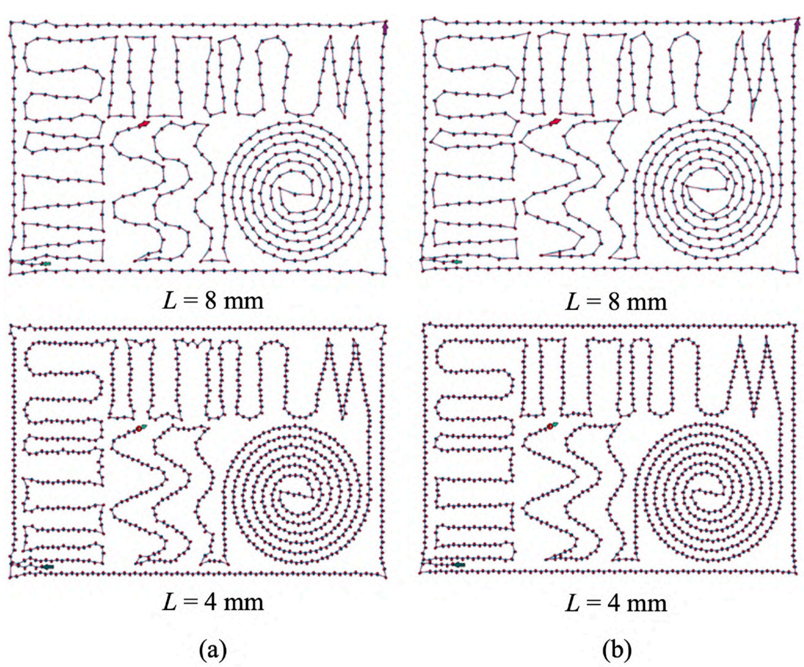

Fig. 14. Comparison of the updated corrected path considering (a) forward and (b) inverted methods for correcting the target path, with L = 8 mm on the top and L = 4 mm on the bottom.

local conditions and material changes.

The proposed methodology not only allows for the production of TFP preforms with higher accuracy, increasing the process quality and reliability, but also allows the usage of high stitching speeds, keeping acceptable accuracy and increasing industrial production. The differences in the width observed in the regions with high deviations change the height of the preforms, an effect that scales up when stacking layers of preforms. This effect could also be mitigated by applying a corrected path. Although the digitalization process applied here was performed in a flatbed scanner, it could be conducted by coupling a measuring system next to the machine's head, speeding up the process and favoring industrial applications. From the sensitivity analysis performed here, it is clear that the TFP process has plenty of room for improvement regarding the production time/accuracy ratio when balancing the stitching speed and the position of stitching points. However, this subject is beyond the scope of the present work.

CRediT authorship contribution statement

Eduardo A.W. de Menezes: Writing – original draft, Visualization, Validation, Methodology, Investigation. **Lars Bittrich:** Writing – review & editing, Software, Project administration, Methodology, Investigation, Conceptualization. **Patrick Schiebel:** Supervision, Funding acquisition, Conceptualization. **Andrea Miene:** Writing – review & editing, Validation, Software, Project administration, Data curation. **Leonel Echer:** Writing – review & editing, Supervision, Funding acquisition. **Mareike Woestmann:** Validation, Investigation. **Axel Spickenheuer:** Writing – review & editing, Visualization, Project administration, Funding acquisition, Formal analysis, Conceptualization.

Declaration of competing interest

The authors declare the following financial interests/personal relationships which may be considered as potential competing interests: Eduardo Antonio Wink de Menezes reports financial support was provided by Federal Ministry for Economic Affairs and Climate Protection, German Bundestag. If there are other authors, they declare that they have no known competing financial interests or personal relationships that could have appeared to influence the work reported in this paper.

Acknowledgments

This work was founded by the Federal Ministry for Economic Affairs and Climate Protection based on a resolution of the German Bundestag, under the CORNET initiative, project number 316 EBG. The authors would also like to thank IPF technicians Nicole Schmidt and Richard Jarosik for their relentless effort in stitching hundreds of training tracks.

Data availability

Data will be made available on request.

References

[1] S.W. Tsai, HT. Hahn, Introduction to Composite Materials, Technomic, Lancaster, 1980.
[2] EJ. Barbero, Introduction to Composite Materials Design, 3rd ed., Taylor & Francis, Boca Raton, 2018.
[3] B. Sobhani Aragh, E. Borzabadi Farahani, B.X. Xu, H. Ghasemnejad, W.J. Mansur, Manufacturable insight into modelling and design considerations in fibre-steered composite laminates: state of the art and perspective, Comput. Methods Appl. Mech. Eng. 379 (2021) 113752, https://doi.org/10.1016/j.cma.2021.113752.
[4] L. Zhang, X. Wang, J. Pei, Y. Zhou, Review of automated fibre placement and its prospects for advanced composites, J. Mater. Sci. 55 (2020) 7121–7155, https://doi.org/10.1007/s10853-019-04090-7.
[5] Y. Li, C. Zheng, J. Jiang, H. Wang, W. Zhu, Q. Wang, et al., Numerical and experimental study of the viscosity and mechanical parameters effect on tow feeding quality during automated fiber placement, J. Manuf. Process. 96 (2023) 31–40, https://doi.org/10.1016/j.jmapro.2023.04.048.
[6] R.R. Dos Santos, S.G.P. Castro, Lightweight design of variable-stiffness cylinders with reduced imperfection sensitivity enabled by continuous tow shearing and machine learning, Materials. (Basel) 15 (2022) 4117, https://doi.org/10.3390/ma15124117.
[7] B.C. Kim, K. Potter, PM. Weaver, Continuous tow shearing for manufacturing variable angle tow composites, Compos. Part a Appl. Sci. Manuf. 43 (2012) 1347–1356, https://doi.org/10.1016/j.compositesa.2012.02.024.
[8] P. Mattheij, K. Gliesche, D. Feltin, 3D reinforced stitched carbon/epoxy laminates made by tailored fibre placement, Compos. Part a Appl. Sci. Manuf. 31 (2000) 571–581, https://doi.org/10.1016/S1359-835X(99)00096-2.
[9] A. Spickenheuer, M. Schulz, K. Gliesche, G. Heinrich, Using tailored fibre placement technology for stress adapted design of composite structures, Plast Rubber Compos 37 (2008) 227–232, https://doi.org/10.1179/174328908X309448.
[10] P.J. Crothers, K. Drechsler, D. Feltin, I. Herszberg, T. Kruckenberg, Tailored fibre placement to minimise stress concentrations, Compos. Part a Appl. Sci. Manuf. 28 (1997) 619–625, https://doi.org/10.1016/S1359-835X(97)00022-5.
[11] J. Simon, N. Hamila, C. Binetruy, S. Comas-Cardona, B. Masseteau, Design and numerical modelling strategy to form tailored fibre placement preforms: application to the tetrahedral part with orthotropic final configuration, Compos. Part a Appl. Sci. Manuf. 158 (2022) 106952, https://doi.org/10.1016/j.compositesa.2022.106952.
[12] L. Bittrich, A. Spickenheuer, J.H.S. Almeida, S. Müller, L. Kroll, G. Heinrich, Optimizing variable-axial Fiber-reinforced composite laminates: the direct Fiber path optimization concept, Math. Probl. Eng. 2019 (2019), https://doi.org/10.1155/2019/8260563.
[13] N.A. Warrior, C.D. Rudd, SP. Gardner, Experimental studies of embroidery for the local reinforcement of composites structures: 1. Stress concentrations, Compos. Sci. Technol. 59 (1999) 2125–2137, https://doi.org/10.1016/s0266-3538(99)00071-8.
[14] S. Spitzer, A. Dargel, J. Kluger, A. Spickenheuer, Design, modelling and manufacturing of a variable-axial composite structural guide Vane for a jet engine intermediate case in the context of industry 4.0, in: SAMPE Eur. Conf., Baden /Zürich - Switzerland, 2021, pp. 1–9.
[15] K. Uhlig, L. Bittrich, A. Spickenheuer, JHS. Almeida, Waviness and fiber volume content analysis in continuous carbon fiber reinforced plastics made by tailored fiber placement, Compos. Struct. 222 (2019) 110910, https://doi.org/10.1016/j.compstruct.2019.110910.
[16] A. Poniecka, M. Barburski, D. Ranz, J. Cuartero, R. Miralbes, Comparison of mechanical properties of composites reinforced with technical embroidery, UD and woven fabric made of flax fibers, Materials. (Basel) 15 (2022) 7469, https://doi.org/10.3390/ma15217469.
[17] E. Richter, A. Spickenheuer, L. Bittrich, K. Uhlig, G. Heinrich, Mechanical design of intersection points of tailored fiber placement made carbon fiber reinforced plastic truss-like structures, Key. Eng. Mater. 809 (KEM) (2019) 452–460, https://doi.org/10.4028/www.scientific.net/KEM.809.452.
[18] K. Uhlig, A. Spickenheuer, K. Gliesche, I. Karb, Strength of CFRP open hole laminates made from NCF, TFP and braided preforms under cyclic tensile loading, Plast Rubber Compos 39 (2010) 247–255, https://doi.org/10.1179/174328910X12647080902772.
[19] K. Uhlig, M. Tosch, L. Bittrich, A. Leipprand, S. Dey, A. Spickenheuer, et al., Meso-scaled finite element analysis of fiber reinforced plastics made by Tailored Fiber Placement, Compos. Struct. 143 (2016) 53–62, https://doi.org/10.1016/j.compstruct.2016.01.049.
[20] D. Chung, P. Jeong, D. Kwon, H. Han, Technology acceptance prediction of robo-advisors by machine learning, Intell Syst. with Appl. 18 (2023) 200197, https://doi.org/10.1016/j.iswa.2023.200197.
[21] T. Jiang, J.L. Gradus, AJ. Rosellini, Supervised machine learning: a brief primer, Behav. Ther. 51 (2020) 675–687, https://doi.org/10.1016/j.beth.2020.05.002.
[22] I. Bahiuddin, J. Fatr, R. Milde, V. Pata, U. Ubaidillah, S.A. Mazlan, et al., Machine learning-based surface roughness prediction in magnetorheological finishing of polyamide influenced by initial conditions, J. Manuf. Process. 145 (2025) 440–453, https://doi.org/10.1016/j.jmapro.2025.04.074.
[23] W. Liu, J. Fang, S. Rolfo, C. Moulinec, DR. Emerson, On the improvement of the extrapolation capability of an iterative machine-learning based RANS Framework, Comput. Fluids. 256 (2023) 105864, https://doi.org/10.1016/j.compfluid.2023.105864.
[24] C.E. Okafor, S. Iweriolor, O.I. Ani, S. Ahmad, S. Mehfuz, G.O. Ekwueme, et al., Advances in machine learning-aided design of reinforced polymer composite and hybrid material systems, Hybrid Adv. 2 (2023) 100026, https://doi.org/10.1016/j.hybadv.2023.100026.
[25] J V Tu, Advantages and disadvantages of using artificial neural networks versus logistic regression for predicting medical outcomes, J. Clin. Epidemiol. 49 (1996) 1225–1231, https://doi.org/10.1016/S0895-4356(96)00002-9.
[26] T. Kunishima, Y. Nagai, G. Bouvard, J.C. Abry, V. Fridrici, P. Kapsa, Comparison of the tribological properties of carbon/glass fiber reinforced PA66-based composites in contact with steel, with and without grease lubrication, Wear. 477 (2021) 203899, https://doi.org/10.1016/j.wear.2021.203899.
[27] BL. Welch, The significance of The difference between two means when The population variances are unequal, Biometrika 29 (1938) 350–362, https://doi.org/10.1093/biomet/29.3-4.350.